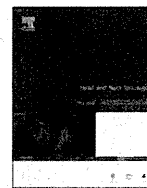


- formation and endochondral ossification. *Development* 137, 901–911.
- Heasman, S.J., Ridley, A.J., 2008. Mammalian Rho GTPases: new insights into their functions from in vivo studies. *Nat. Rev. Mol. Cell Biol.* 9, 690–701.
- Hernandez-Martinez, R., Covarrubias, L., 2011. Interdigital cell death function and regulation: new insights on an old programmed cell death model. *Dev. Growth Differ.* 53, 245–258.
- Houzelstein, D., Cohen, A., Buckingham, M.E., Robert, B., 1997. Insertional mutation of the mouse *Msx1* homeobox gene by an *nlacZ* reporter gene. *Mech. Dev.* 65, 123–133.
- Ito, Y., Teitelbaum, S.L., Zou, W., Zheng, Y., Johnson, J.F., Chappel, J., Ross, F.P., Zhao, H., 2010. *Cdc42* regulates bone modeling and remodeling in mice by modulating RANKL/M-CSF signaling and osteoclast polarization. *J. Clin. Invest.* 120, 1981–1993.
- Karsenty, G., 2003. The complexities of skeletal biology. *Nature* 423, 316–318.
- Kronenberg, H.M., 2003. Developmental regulation of the growth plate. *Nature* 423, 332–336.
- LaLonde, D.P., Grubinger, M., Lamarche-Vane, N., Turner, C.E., 2006. *CdGAP* associates with actopaxin to regulate integrin-dependent changes in cell morphology and motility. *Curr. Biol.* 16, 1375–1385.
- Logan, M., Martin, J.F., Nagy, A., Lobe, C., Olson, E.N., Tabin, C.J., 2002. Expression of Cre recombinase in the developing mouse limb bud driven by a *Prx1* enhancer. *Genesis* 33, 77–80.
- Maatouk, D.M., Choi, K.S., Bouldin, C.M., Harfe, B.D., 2009. In the limb AER *Bmp2* and *Bmp4* are required for dorsal-ventral patterning and interdigital cell death but not limb outgrowth. *Dev. Biol.* 327, 516–523.
- Macias, D., Ganan, Y., Sampath, T.K., Piedra, M.E., Ros, M.A., Hurle, J.M., 1997. Role of BMP-2 and OP-1 (BMP-7) in programmed cell death and skeletogenesis during chick limb development. *Development* 124, 1109–1117.
- Melendez, J., Grogg, M., Zheng, Y., 2011. Signaling role of *Cdc42* in regulating mammalian physiology. *J. Biol. Chem.* 286, 2375–2381.
- Merino, R., Macias, D., Ganan, Y., Economides, A.N., Wang, X., Wu, Q., Stahl, N., Sampath, K.T., Varona, P., Hurle, J.M., 1999. Expression and function of *Gdf-5* during digit skeletogenesis in the embryonic chick leg bud. *Dev. Biol.* 206, 33–45.
- Niswander, L., 2003. Pattern formation: old models out on a limb. *Nat. Rev. Genet.* 4, 133–143.
- Oldfield, S.F., Evans, D.J., 2003. Tendon morphogenesis in the developing avian limb: plasticity of fetal tendon fibroblasts. *J. Anat.* 202, 153–164.
- Ovchinnikov, D.A., Selever, J., Wang, Y., Chen, Y.T., Mishina, Y., Martin, J.F., Behringer, R.R., 2006. BMP receptor type IA in limb bud mesenchyme regulates distal outgrowth and patterning. *Dev. Biol.* 295, 103–115.
- Pizette, S., Abate-Shen, C., Niswander, L., 2001. BMP controls proximodistal outgrowth, via induction of the apical ectodermal ridge, and dorsoventral patterning in the vertebrate limb. *Development* 128, 4463–4474.
- Robert, B., 2007. Bone morphogenetic protein signaling in limb outgrowth and patterning. *Dev. Growth Differ.* 49, 455–468.
- Rodriguez, C.I., Buchholz, F., Galloway, J., Sequerra, R., Kasper, J., Ayala, R., Stewart, A.F., Dymecki, S.M., 2000. High-efficiency deleter mice show that *FLPe* is an alternative to *Cre-loxP*. *Nat. Genet.* 25, 139–140.
- Sagai, T., Hosoya, M., Mizushina, Y., Tamura, M., Shiroishi, T., 2005. Elimination of a long-range cis-regulatory module causes complete loss of limb-specific *Shh* expression and truncation of the mouse limb. *Development* 132, 797–803.
- Shaheen, R., Faqeih, E., Sunker, A., Morsy, H., Al-Sheddi, T., Shamseldin, H.E., Adly, N., Hashem, M., Alkuraya, F.S., 2011. Recessive mutations in *DOCK6*, encoding the guanidine nucleotide exchange factor *DOCK6*, lead to abnormal actin cytoskeleton organization and Adams–Oliver syndrome. *Am. J. Hum. Genet.* 89, 328–333.
- Shapiro, I.M., Adams, C.S., Freeman, T., Srinivas, V., 2005. Fate of the hypertrophic chondrocyte: microenvironmental perspectives on apoptosis and survival in the epiphyseal growth plate. *Birth Defects Res. C Embryo Today* 75, 330–339.
- Soriano, P., 1999. Generalized *lacZ* expression with the ROSA26 Cre reporter strain. *Nat. Genet.* 21, 70–71.
- Southgate, L., Machado, R.D., Snape, K.M., Primeau, M., Dafou, D., Ruddy, D.M., Branney, P.A., Fisher, M., Lee, G.J., Simpson, M.A., He, Y., Bradshaw, T.Y., Blaumeiser, B., Winship, W.S., Reardon, W., Maher, E.R., Fitzpatrick, D.R., Wuyts, W., Zenker, M., Lamarche-Vane, N., Trembath, R.C., 2011. Gain-of-function mutations of *ARHGAP31*, a *Cdc42/Rac1* GTPase regulator, cause syndromic cutis aplasia and limb anomalies. *Am. J. Hum. Genet.* 88, 574–585.
- Spagnoli, A., O'Rear, L., Chandler, R.L., Granero-Molto, F., Mortlock, D.P., Gorska, A.E., Weis, J.A., Longobardi, L., Chytil, A., Shimer, K., Moses, H.L., 2007. TGF-beta signaling is essential for joint morphogenesis. *J. Cell Biol.* 177, 1105–1117.
- Suzuki, D., Yamada, A., Amano, T., Yasuhara, R., Kimura, A., Sakahara, M., Tsumaki, N., Takeda, S., Tamura, M., Nakamura, M., Wada, N., Nohno, T., Shiroishi, T., Aiba, A., Kamijo, R., 2009. Essential mesenchymal role of small GTPase *Rac1* in interdigital programmed cell death during limb development. *Dev. Biol.* 335, 396–406.
- Tickle, C., 2002. Molecular basis of vertebrate limb patterning. *Am. J. Med. Genet.* 112, 250–255.
- Wang, G., Beier, F., 2005. *Rac1/Cdc42* and *RhoA* GTPases antagonistically regulate chondrocyte proliferation, hypertrophy, and apoptosis. *J. Bone Miner. Res.* 20, 1022–1031.
- Woods, A., Wang, G., Beier, F., 2007a. Regulation of chondrocyte differentiation by the actin cytoskeleton and adhesive interactions. *J. Cell. Physiol.* 213, 1–8.
- Woods, A., Wang, G., Dupuis, H., Shao, Z., Beier, F., 2007b. *Rac1* signaling stimulates N-cadherin expression, mesenchymal condensation, and chondrogenesis. *J. Biol. Chem.* 282, 23500–23508.
- Yamada, A., Sheikh, F., Niimi, T., DeMayo, F.J., Keegan, A.D., Donnelly, R.P., Kimura, S., 2005. Induction of uteroglobin-related protein 2 (*Ugrp2*) gene expression by the Th2 cytokines IL-4 and IL-13. *J. Immunol.* 175, 5708–5715.
- Zanetti, N.C., Solursh, M., 1984. Induction of chondrogenesis in limb mesenchymal cultures by disruption of the actin cytoskeleton. *J. Cell Biol.* 99, 115–123.
- Zhang, X., Siclari, V.A., Lan, S., Zhu, J., Koyama, E., Dupuis, H.L., Enomoto-Iwamoto, M., Beier, F., Qin, L., 2011. The critical role of the epidermal growth factor receptor in endochondral ossification. *J. Bone Miner. Res.* 26, 2622–2633.
- Zou, H., Wieser, R., Massague, J., Niswander, L., 1997. Distinct roles of type I bone morphogenetic protein receptors in the formation and differentiation of cartilage. *Genes Dev.* 11, 2191–2203.



Clinical significance of lymphatic and blood vessel invasion in oral tongue squamous cell carcinomas

Chieko Michikawa^{a,b}, Narikazu Uzawa^{a,*}, Kou Kayamori^{b,c}, Itaru Sonoda^a, Yoshio Ohyama^a, Norihiko Okada^b, Akira Yamaguchi^d, Teruo Amagasa^a

^a Maxillofacial Surgery, Maxillofacial Reconstruction and Function, Division of Maxillofacial and Neck Reconstruction, Graduate School of Medical and Dental Sciences, Tokyo Medical and Dental University, Tokyo, Japan

^b Diagnostic Oral Pathology, Oral Restitution, Division of Oral Health Sciences, Graduate School of Medical and Dental Sciences, Tokyo Medical and Dental University, Tokyo, Japan

^c Department of Pathology, Ome Municipal General Hospital, Ome, Tokyo, Japan

^d Oral Pathology, Oral Restitution, Division of Oral Health Sciences, Graduate School of Medical and Dental Sciences, Tokyo Medical and Dental University, Tokyo, Japan

ARTICLE INFO

Article history:

Received 12 September 2011

Received in revised form 14 November 2011

Accepted 20 November 2011

Available online 16 December 2011

Keywords:

Lymphatic vessel invasion

Blood vessel invasion

Oral tongue

Squamous cell carcinoma

D2-40

Elastica van Gieson stain

Lymph node

Metastasis

Prognosis

SUMMARY

Although vascular invasion (VI) is recognized as an important predictor of lymph node metastasis and a significant prognostic factor in head and neck squamous cell carcinoma (HNSCC), there is currently no common definition for the pathological evaluation of VI status. We reviewed the medical records of 63 consecutive resected primary oral tongue SCCs (OTSCCs) without preoperative treatment between June 1999 and April 2008, and evaluated VI status by investigating lymphatic vessel invasion (LVI) and blood vessel invasion (BVI) by using immunohistochemistry (IHC) with monoclonal antibody D2-40 (D2-40) and Elastica van Gieson (EVG) staining, respectively. Subsequently, we analyzed their correlations with cervical lymph node metastasis and prognosis. LVI was found in 16 of the 63 tumors (25.4%) and BVI was in 32 tumors (50.8%). Univariate analysis revealed that the presence of LVI is statistically correlated with lymph node metastasis. Moreover, multivariate logistic regression analysis revealed that LVI is an independent risk factor of nodal metastasis (odds ratio = 4.262, 95% confidence interval = 1.262–14.397, $p = 0.020$). In contrast, Kaplan–Meier survival analysis revealed that patients with BVI had a significantly shorter disease-free survival (DFS) and overall survival (OS) rates than those without BVI (68.6% versus 90.3%, $p = 0.028$ and 68.6% versus 93.5%, $p = 0.013$, respectively). The present study clearly demonstrated that LVI at primary OTSCC had significant correlation with lymph node metastasis, and that BVI was significantly associated with recurrence and poor prognosis. Evaluation of VI status, as LVI and BVI status separately, using IHC with D2-40 and EVG staining may be useful in predicting lymph node metastasis and poor prognosis in OTSCCs.

© 2011 Elsevier Ltd. All rights reserved.

Introduction

It is generally accepted that tumor invasion to vascular is the first step in the development of a metastatic focus in general solid malignant tumors. Vascular invasion (VI) includes lymphatic vessel invasion (LVI) and blood vessel invasion (BVI), both of which are thought to be the beginning of lymphogenous and hematogenous metastasis, respectively.^{1,2}

The importance of LVI in lymph node metastasis and prognosis in various kinds of solid tumor is clearly recognized.^{1,3–9} However, little attention has been placed upon VI in relation to oral malignancies and the development of lymph node metastasis and prognosis. One of the main reasons for this may be that interobserver variability in the evaluation of LVI and BVI cannot be neglected because of the difficulties in recognizing lymphatic channels and veins using standard hematoxylin and eosin (HE) staining alone.^{10–13}

Recently, immunohistochemistry (IHC) and special staining for identifying lymphatic channels and vessels have been widely used to determine VI in various tumors.^{10–15} For example, IHC with the monoclonal antibody D2-40 (D2-40) not only highlights lymphatic channels, but this antibody also reacts with O-linked sialoglycoprotein (MW: 40 kda) on the surface of the lymphatic endothelium, making it a new selective marker that enables us to distinguish lymphatic channels from vessels.^{12–14,16} Identification of vessels has been further aided by Elastica van Gieson (EVG) staining,

* Corresponding author. Address: Maxillofacial Surgery, Maxillofacial Reconstruction and Function, Division of Maxillofacial and Neck Reconstruction, Graduate School of Medical and Dental Sciences, Tokyo Medical and Dental University, 1-5-45 Yushima, Bunkyo-ku, Tokyo 113-8549, Japan. Tel.: +81 3 5803 5499; fax: +81 3 5803 5500.

E-mail addresses: c-michikawa.mfs@tmd.ac.jp (C. Michikawa), n-uzawa.mfs@tmd.ac.jp (N. Uzawa), kayamori.mpa@tmd.ac.jp (K. Kayamori), italu_mfs@yahoo.co.jp (I. Sonoda), yohyama1219@gmail.com (Y. Ohyama), nokd.opth@tmd.ac.jp (N. Okada), akira.mpa@tmd.ac.jp (A. Yamaguchi), amagasa.mfs@tmd.ac.jp (T. Amagasa).

which stains elastic fibers located in the venous wall dark violet. Thus, EVG staining significantly improve the accuracy of BVI evaluation.^{15,17–19}

In this study, we therefore attempted to evaluate the VI status of oral tongue squamous cell carcinomas (OTSCCs) by investigating LVI status using IHC with D2-40 and BVI status using EVG staining of primary OTSCCs, and we subsequently examined the association between VI status and cervical lymph node metastasis and prognosis.

Materials and methods

Materials

The medical records of 63 consecutive OTSCC patients who had undergone curative surgery at Maxillofacial Surgery, University Hospital of Dentistry, Tokyo Medical and Dental University (Tokyo, Japan), between June 1999 and April 2008 were reviewed for this study. No patients underwent preoperative treatment. All protocols were reviewed and approved by the Research Ethics Committee of Tokyo Medical and Dental University, and informed consent was obtained from all patients in accordance with our Institutional guidelines. Detailed patient characteristics are described in Table 1. Primary tumors were resected then immediately fixed in 10% (v/v) formalin and embedded in paraffin. Serial 4- μ m sections were prepared from each sample for routine HE staining to obtain pathological information (Tables 1). Pathological T staging, cellular differentiation and the mode of invasion of primary tumors were defined on the basis of the International Union Against Cancer TNM classification,²⁰ the World Health Organization (WHO) classification,²¹ and the modification of the criteria of Jakobsson et al.,^{22,23} respectively. Pathological data included LVI and BVI in primary tumors. One or two (mean: 1.6) additional paraffin blocks of aggressive sections were used for IHC with D2-40 and EVG staining to evaluate LVI and BVI, respectively.

Table 1
Correlation between LVI/BVI and clinicopathological parameters.

Clinicopathological parameters	LVI+	LVI–	P value	BVI+	BVI–	P value
Gender						
Male	12	37	NS	25	24	NS
Female	4	10		7	7	
Age (yrs)						
\leq 58	6	22	NS	15	13	NS
>58	10	25		17	18	
Growth pattern						
Superficial	1	9	NS	3	7	NS
Exophytic	7	19		11	15	
Endophytic	8	19		18	9	
Pathological T stage						
1–2	13	41	NS	26	28	NS
3	3	6		6	3	
Cellular differentiation						
Well/ Moderate	15	39	NS	26	28	NS
Poor	1	8		6	3	
Mode of invasion						
1–3	9	31	NS	15	25	0.005
4C–4D	7	16		17	6	
Pathological lymph node metastasis						
Negative	5	31	0.015	16	20	NS
Positive	11	16		16	11	
Recurrence/Metastasis						
Negative	13	37	NS	22	28	0.034
Positive	3	10		10	3	
Survival						
Alive	12	39	NS	22	29	0.012
Dead	4	8		10	2	

LVI: lymphatic vessel invasion, BVI: blood vessel invasion, NS: not significant.

Immunohistochemistry and Elastica van Gieson staining

Paraffin sections measuring 4 μ m in thickness were dewaxed and hydrated, then after inactivation of endogenous peroxidase with 3% hydrogen peroxidase for 20 min, they were reacted with anti D2-40 monoclonal antibody (prediluted) (COVANCE, CA) overnight at 4 °C. This was followed by incubation with secondary antibodies (Envision+; Dako, CA). The reaction was visualized using 3,3-diaminobenzidine, and nuclei were lightly counterstained with hematoxylin. LVI positive was defined as the presence of tumor cell aggregates within the D2-40 stained lymphatic lumen or invasion of the media of a vessel with ulceration of the intima (Fig. 1B). It is easier and more accurate to detect LVI using D2-40 than HE staining (Fig. 1A and B).

EVG staining was performed according to the standard protocol. BVI was easily identified with EVG staining because the elastic fiber of the veins was stained dark violet (Fig. 1C and D). BVI positive was defined as the presence of tumor cell aggregates within the dark violet stain or invasion of the media of a vessel with ulceration of the intima (Fig. 1D).

All slides were evaluated independently by two authors (C.M. and K.K.), neither of whom had knowledge of the clinical data. LVI and BVI were considered positive only when both observers agreed.

Statistical analysis

VI status was compared with the patient's clinicopathological information using the chi-square test. After initial screening by univariate analysis, multivariate logistic regression analysis was applied to analyze the significant risk factors of lymph node metastasis. The disease-free survival (DFS) rate and overall survival (OS) rate were estimated using the Kaplan–Meier method and statistical significance was determined using the log-rank test. DFS time was defined as the interval between the date of first visit and the date of development of local, regional recurrence and distant metastasis after surgery. OS time was also calculated from the date of initial examination to the date of death, or to the date of the five-year follow-up. All statistical analyses were performed using SPSS for Windows (version 17.0, SPSS, Inc., Chicago, IL). *P* values less than 0.05 were considered statistically significant.

Results

Clinicopathological data

Patients included 49 males (77.8%) and 14 females (22.2%) with a mean age of 57.9 years (range, 20–89). The median follow-up period was 41.5 months (range, 8.3–60.0). The growth pattern of the primary tumor was classified as superficial ($n = 10$, 15.9%), exophytic ($n = 26$, 41.3%), or endophytic ($n = 27$, 42.8%). Of the 63 patients, 23 (36.5%) presented with T1, 31 (49.2%) with T2, 9 (14.3%) with T3 tumors. Of the 63 patients, 27 (42.9%) had positive nodes.

Staining

To evaluate the presence of LVI and BVI in primary OTSCCs, IHC with D2-40 and EVG staining were performed (Fig. 1). LVI is found in 16 of the 63 tumors (25.4%), and BVI is found in 32 (50.8%).

Association with clinicopathological parameters

The association between LVI/BVI status and the clinicopathological parameters in the OTSCC patients are summarized in Table 1. There were no significant correlations between LVI and gender,

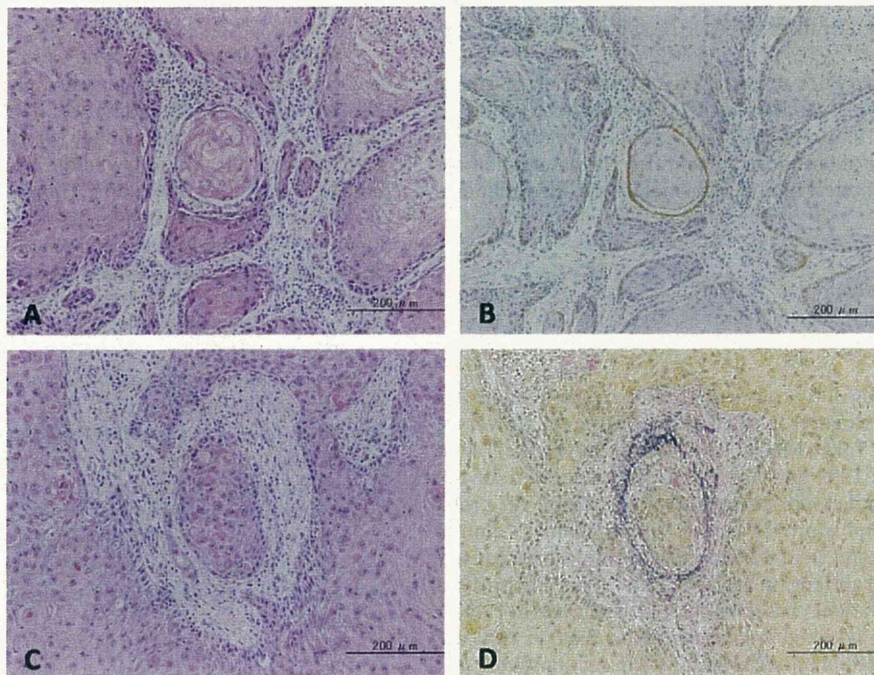


Figure 1 Lymphatic vessel invasion and blood vessel invasion (original magnification: 100 \times). (A) It is difficult to judge lymphatic vessel invasion (LVI) on HE staining. (B) LVI is easily identified because the lymphatic endothelium is highlighted with D2-40 staining. (C) It is difficult to identify blood vessel invasion (BVI) on HE staining. (D) BVI is easily identified because the elastic fiber of the vein is stained dark violet with EVG staining.

age, growth pattern, pathological T stage, cellular differentiation, mode of invasion, and disease recurrence or survival. In contrast, LVI was significantly correlated with lymph node metastasis ($p = 0.015$).

On the other hand, although BVI was not associated with lymph node metastasis, BVI was significantly associated with mode of invasion ($p = 0.005$), disease recurrence ($p = 0.034$) and survival ($p = 0.012$).

LVI impact on lymph node metastasis

To investigate the risk factors of lymph node metastasis, multivariate logistic regression analysis was conducted with gender, age, pathological T stage, cellular differentiation, mode of invasion, and the LVI/BVI status of the primary OTSCCs as variables. As a result, LVI was shown to be a significant independent risk factor of lymph node metastasis (odds ratio = 4.262, 95% confidence interval = 1.262–14.397, $p = 0.020$; Table 2).

BVI impact on recurrence and survival

To assess the impact of LVI or BVI status on survival, survival data was compared between the groups, those that were LVI/BVI positive and negative, respectively. Kaplan–Meier survival curves

Table 2
Independent risk factor of pN in multivariate logistic regression analysis.

Variables	OR	95% CI	P value
Gender	–	–	NS
Age	–	–	NS
Pathological T stage	–	–	NS
Cellular differentiation	–	–	NS
Mode of invasion	–	–	NS
LVI	4.262	1.262–14.397	0.02
BVI	–	–	NS

pN: pathological lymph node metastasis, OR: odds ratio, CI: confidence interval, LVI: lymphatic vessel invasion, BVI: blood vessel invasion.

for DFS and OS are presented in Fig. 2. With regard to LVI status, five-year DFS rates were 78.7% for LVI negative and 80.8% for LVI positive patients. Five-year OS rates were 83.0% for LVI negative and 75.0% for LVI positive patients. Therefore, LVI status has a little or no effect on both DFS and OS in OTSCCs. On the contrary, five-year DFS and OS rates were significantly lower in patients with BVI positive tumors than those with negative tumors (68.6% versus 90.3%, $p = 0.028$ and 68.6% versus 93.5%, $p = 0.013$, respectively), suggesting that the presence of BVI may have an adverse impact on the DFS and OS in OTSCCs.

Discussion

Although VI is recognized as an important predictor of lymph node metastasis and a significant prognostic factor in HNSCC, there is currently no common definition for the pathological evaluation of

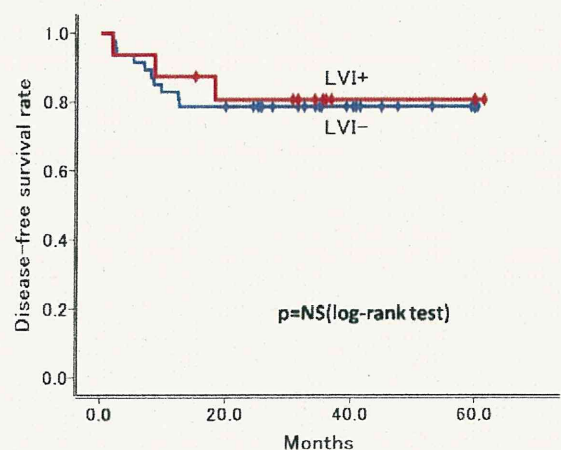


Figure 2A Kaplan–Meier curve for disease-free survival according to LVI status.

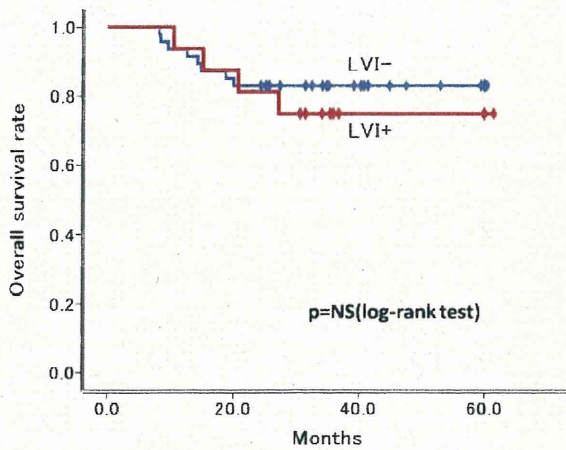


Figure 2B Kaplan–Meier curve for overall survival according to LVI status.

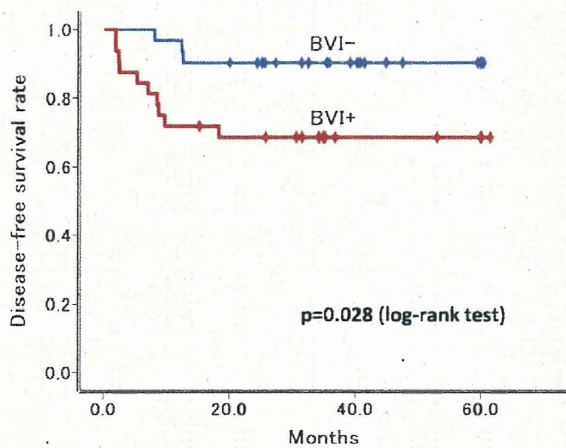


Figure 2C Kaplan–Meier curve for disease-free survival according to BVI status.

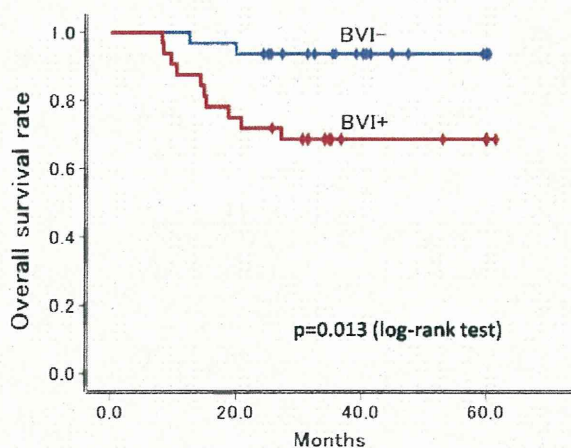


Figure 2D Kaplan–Meier curve for overall survival according to BVI status.

VI status.^{24–28} One of the main reasons is that interobserver discrepancy cannot be neglected, and such discordance may result from difficulties in evaluating VI status by conventional HE staining alone. Several studies have revealed diagnostic inconsistency between conventional HE staining and IHC with D2-40 or EVG staining for the evaluation of pathological state.^{11–13} Using a series

comprising 221 stage IA non-small cell lung cancers, Hashizume et al.¹³ found that HE staining showed both many false-negative results and false-positive results compared with D2-40 immunostaining in detection of LVI. In addition, Saad et al.¹² reported that using D2-40 instead of HE staining increased detection of LVI in colorectal cancers. Moreover, investigating BVI status in 124 T1 colorectal cancer specimens, Suzuki et al.¹¹ concluded that EVG staining significantly increases the positivity rate for BVI and reduces interobserver discrepancies. These findings suggest that VI status should be evaluated by LVI and BVI using IHC with monoclonal antibody D2-40 and EVG staining, respectively, to evaluate VI status precisely and to minimize interobserver variability. Therefore, in the present study, we attempted to precisely evaluate the VI status of OTSCCs according to the above-mentioned methods. Subsequently, we clearly demonstrated that LVI is a risk factor for cervical lymph node metastasis and that the presence of BVI correlates significantly with recurrence and poor prognosis in patients with OTSCCs. To our knowledge, this is the first study to precisely evaluate LVI and BVI separately in primary OTSCCs and reveal the significant correlation between status and clinicopathological factors.

Several studies on VI status and its correlation with clinicopathological factors in HNSCC have been published. In 1987, Close et al.²⁴ found a highly significant correlation between the presence of VI (LVI and/or BVI) in the primary tumor and the development of cervical lymph node metastasis in 43 HNSCC patients. This is the first report that showed a statistically significant relationship between VI status and lymph node metastasis in HNSCCs. A similar finding was reported by Woolgar et al.²⁶ in which logistic regression analysis of 45 OSCC patients revealed that VI was a significant predictor of nodal metastasis. More recently, Jones et al.²⁷ investigated 72 OSCC patients using univariate analysis and found that LVI, not VI, correlated significantly with lymph node metastasis. In the present study, we retrospectively examined 63 patients with OTSCCs, and univariate analysis revealed that LVI significantly correlates with lymph node metastasis. Moreover, multivariate logistic regression analysis showed that the presence of LVI is an independent risk factor of nodal metastasis. Although direct comparison with previous reports regarding VI status in HNSCCs should be performed with caution, due to the different evaluation methods of VI status (HE staining alone versus IHC and EVG staining), the present results are consistent with previous findings.

Regarding survival, Close et al.²⁵ showed in a series of 65 HNSCC cases that VI correlates with both recurrence and survival. They also revealed that only VI had a significant impact on survival when using multivariate analysis for examining multiple clinicopathological factors. Recently, two different findings were presented. Jones et al.²⁷ investigated LVI status, not VI status, and following multivariate analysis reported that the presence of LVI had the greatest impact on survival in 72 OSCC patients. On the other hand, Rahima et al.²⁸ showed that LVI did not correlate with recurrence and survival in 101 HNSCC cases. These controversial results may be the result of the difficulty of the precise evaluation of LVI/BVI status by conventional HE staining alone. Thus, in this study, we tried to evaluate the LVI/BVI status of OTSCCs using IHC and special staining. Consequently, we clearly demonstrated that LVI status correlates significantly with lymph node metastasis and that BVI status has a significant adverse impact on recurrence and survival in OTSCC cases, suggesting that the status of LVI and BVI is related to different clinical factors. These observations indicate the importance of separately evaluating LVI and BVI status using IHC and special staining.

As expected, we showed that LVI, but not BVI, was significantly associated with the presence of lymph node metastasis in patients with OTSCC by univariate and multivariate analysis. Based on the hypothesis that LVI at the primary site is the first step in the development of a cervical metastatic focus, this finding seems to be re-

sonable.^{1,2} Of particular interest, although BVI was not correlated with hematogenous spread such as distant metastasis (data not shown), Kaplan–Meier survival analysis revealed that patients with BVI had a significantly shorter DFS and OS. This observation showed the difference feature between cancer cells which can invade blood and lymphatic vessels. In general, there are anatomical differences in the walls of blood and lymphatic vessels. Blood vessels have elastic fiber and muscle in their wall, whereas lymphatic vessels consist of epithelial cells.^{2,29,30} Thus, when cancer cells invade blood vessels, they can penetrate the basement membrane and migrate through the endothelial tight junctions of the vessel.^{2,29} Therefore, these cancer cells are more aggressive in nature, and the presence of BVI at the primary site may be a significant marker for tumor aggressiveness.

In conclusion, LVI at the primary site evaluated by IHC with D2-40 was significantly associated with cervical lymph node metastasis. In addition, the presence of BVI evaluated by EVG staining correlated with poor outcome in OTSCC patients. Evaluation of VI status using IHC with D2-40 and EVG staining may be useful for predicting lymph node metastasis and poor prognosis in OTSCC cases. To establish a standardized staining protocol and reveal the clinical significance of both LVI and BVI in patients with OTSCC, a larger multicenter prospective study is required.

Conflict of interest statement

None declared.

References

- Liang P, Nakada I, Hong JW, Tabuchi T, Motohashi G, Takemura A, et al. Prognostic significance of immunohistochemically detected blood and lymphatic vessel invasion in colorectal carcinoma: its impact on prognosis. *Ann Surg Oncol* 2007; **14**(2):470–7.
- Stacker SA, Baldwin ME, Achen MG. The role of tumor lymphangiogenesis in metastatic spread. *FASEB J (United States)* 2002; **922**–34.
- Algaba F. Lymphovascular invasion as a prognostic tool for advanced bladder cancer. *Curr Opin Urol (United States)* 2006; **367**–71.
- Kim JM, Kim TY, Kim WB, Gong G, Kim SC, Hong SJ, et al. Lymphovascular invasion is associated with lateral cervical lymph node metastasis in papillary thyroid carcinoma. *Laryngoscope* 2006; **116**(11):2081–5.
- Woo CS, Silberman H, Nakamura SK, Ye W, Sposto R, Colburn W, et al. Lymph node status combined with lymphovascular invasion creates a more powerful tool for predicting outcome in patients with invasive breast cancer. *Am J Surg (United States)* 2002; **337**–40.
- Gurleyik G, Gurleyik E, Aker F, Aktekin A, Emir S, Gungor O, et al. Lymphovascular invasion, as a prognostic marker in patients with invasive breast cancer. *Acta Chir Belg* 2007; **107**(3):284–7.
- Brooks JP, Albert PS, O'Connell J, McLeod DG, Poggi MM. Lymphovascular invasion in prostate cancer: prognostic significance in patients treated with radiotherapy after radical prostatectomy. *Cancer* 2006; **106**(7):1521–6.
- Sakuragi M, Togashi K, Konishi F, Koinuma K, Kawamura Y, Okada M, et al. Predictive factors for lymph node metastasis in T1 stage colorectal carcinomas. *Dis Colon Rectum* 2003; **46**(12):1626–32.
- Tanaka S, Haruma K, Teixeira CR, Tatsuta S, Ohtsu N, Hiraga Y, et al. Endoscopic treatment of submucosal invasive colorectal carcinoma with special reference to risk factors for lymph node metastasis. *J Gastroenterol* 1995; **30**(6):710–7.
- Mohammed RA, Martin SG, Gill MS, Green AR, Paish EC, Ellis IO. Improved methods of detection of lymphovascular invasion demonstrate that it is the predominant method of vascular invasion in breast cancer and has important clinical consequences. *Am J Surg Pathol (United States)* 2007; **1825**–33.
- Suzuki A, Togashi K, Nokubi M, Koinuma K, Miyakura Y, Horie H, et al. Evaluation of venous invasion by Elastica van Gieson stain and tumor budding predicts local and distant metastases in patients with T1 stage colorectal cancer. *Am J Surg Pathol* 2009; **33**(11):1601–7.
- Saad RS, Kordunsky L, Liu YL, Denning KL, Kandil HA, Silverman JF. Lymphatic microvessel density as prognostic marker in colorectal cancer. *Mod Pathol (United States)* 2006; **1317**–23.
- Hashizume S, Nagayasu T, Hayashi T, Hidaka S, Tsuchiya T, Tagawa T, et al. Accuracy and prognostic impact of a vessel invasion grading system for stage IA non-small cell lung cancer. *Lung Cancer (Ireland)* 2009; **363**–70.
- Ishii M, Ota M, Saito S, Kinugasa Y, Akamoto S, Ito I. Lymphatic vessel invasion detected by monoclonal antibody D2-40 as a predictor of lymph node metastasis in T1 colorectal cancer. *Int J Colorectal Dis* 2009; **24**(9):1069–74.
- Sato T, Ueno H, Mochizuki H, Shinto E, Hashiguchi Y, Kajiwara Y, et al. Objective criteria for the grading of venous invasion in colorectal cancer. *Am J Surg Pathol* 2010; **34**(4):454–62.
- Kahn HJ, Marks A. A new monoclonal antibody, D2-40, for detection of lymphatic invasion in primary tumors. *Lab Invest* 2002; **82**(9):1255–7.
- Inoue T, Mori M, Shimono R, Kuwano H, Sugimachi K. Vascular invasion of colorectal carcinoma readily visible with certain stains. *Dis Colon Rectum* 1992; **35**(1):34–9.
- Minsky BD, Mies C, Recht A, Rich TA, Chaffey JT. Resectable adenocarcinoma of the rectosigmoid and rectum. II. The influence of blood vessel invasion. *Cancer* 1988; **61**(7):1417–24.
- Minsky BD, Mies C, Rich TA, Recht A, Chaffey JT. Potentially curative surgery of colon cancer: the influence of blood vessel invasion. *J Clin Oncol* 1988; **6**(1):119–27.
- Sobin LH, Gospodarowicz MK, Wittekind C, editors. *TNM classification of malignant tumors*. 7th ed. New York: Wiley-Blackwell; 2009.
- World Health Organization. International histological classification of tumors, 2nd ed., Springer: Berlin; 1998.
- Yamamoto E, Kohama G, Sunakawa H, Iwai M, Hiratsuka H. Mode of invasion, bleomycin sensitivity, and clinical course in squamous cell carcinoma of the oral cavity. *Cancer* 1983; **51**(12):2175–80.
- Jakobsson PA, Eneroth CM, Killander D, Moberger G, Martensson B. Histologic classification and grading of malignancy in carcinoma of the larynx. *Acta Radiol Ther Phys Biol* 1973; **12**(1):1–8.
- Close LG, Burns DK, Reisch J, Schaefer SD. Microvascular invasion in cancer of the oral cavity and oropharynx. *Arch Otolaryngol Head Neck Surg* 1987; **113**(11):1191–5.
- Close LG, Brown PM, Vuitch MF, Reisch J, Schaefer SD. Microvascular invasion and survival in cancer of the oral cavity and oropharynx. *Arch Otolaryngol Head Neck Surg* 1989; **115**(11):1304–9.
- Woolgar JA, Scott J. Prediction of cervical lymph node metastasis in squamous cell carcinoma of the tongue/floor of mouth. *Head Neck* 1995; **17**(6):463–72.
- Jones HB, Sykes A, Bayman N, Sloan P, Swindell R, Patel M, et al. The impact of lymphovascular invasion on survival in oral carcinoma. *Oral Oncol (England)* 2009; **10**–5.
- Rahima B, Shingaki S, Nagata M, Saito C. Prognostic significance of perineural invasion in oral and oropharyngeal carcinoma. *Oral Surg Oral Med Oral Pathol Oral Radiol Endod (United States)* 2004; **423**–31.
- Swartz MA, Skobe M. *Lymphatic function lymphangiogenesis and cancer metastasis*. Microsc Res Tech., United States: Wiley-Liss, Inc.; 2001. p. 92–9.
- Pepper MS, Tille JC, Nisato R, Skobe M. Lymphangiogenesis and tumor metastasis. *Cell Tissue Res* 2003; **314**(1):167–77.

Ectopic production of hair keratin constitutes Rushton's hyaline bodies in association with hematogenous deposits

Kei Sakamoto, Rumana Khanom, Miwako Hamagaki, Akira Yamaguchi

Sections of Oral Pathology, Tokyo Medical and Dental University, Tokyo, Japan

A Rushton's hyaline body (HB) is a concretion occasionally found in odontogenic cysts. Unspecified substances produced by the lining epithelium or derived from blood components have been suggested as possible causes of HB formation, but the origin of HBs is still elusive. This study aimed to clarify the origin of HBs. Ten specimens with HBs were obtained from 400 odontogenic cysts. HBs were stained by orcein and Congo red. Immunohistochemical examination revealed that HBs were positive for hair keratin and keratin 17. Hair keratin was concentrated in HBs, and cells with hair keratin expression were hardly seen, while cells with keratin 17 expression were observed near HBs. HBs were also positive for hemoglobin alpha chain. The presence of hair keratin in HBs was confirmed by Western blot analysis. The present study suggests that HBs are formed as a consequence of two independent events: unusual alteration of epithelial differentiation so as to provide hair keratin, and hemorrhage so as to provide erythrocytic substances. Although the ectopic production of hair keratin appears more essential, our results reconcile the long-standing debate between two theories, the keratin theory versus the hematogenous theory, concluding that both substances are required for the genesis of HBs, and also suggesting that they might be novel non-pathological amyloidogenic proteins.

J Oral Pathol Med (2012)

Keywords: amyloid; hair keratin; hemoglobin; hyaline bodies; odontogenic cyst; orcein; Rushton bodies

Introduction


The hyaline body (HB), a structure first reported in 1918 by Dewey (1), was described in detail by Rushton (2).

Correspondence: Akira Yamaguchi, Section of Oral Pathology, Tokyo Medical and Dental University, Yushima 1-5-45, Bunkyo-ku, Tokyo 113-0034, Japan. Tel: +81 3 5803 5451, Fax: +81 3 5803 0188, E-mail: akira.mpa@tmd.ac.jp

Accepted for publication March 8, 2012

HBs are hyaline concretions of linear, curved or circular shapes, measuring up to about 0.1 mm in length, and they are found in the lining epithelium of odontogenic cysts (2). They occur in between 4% and 10% of radicular cysts or dentigerous cysts (2–4), producing a positive result with aldehyde fuchsin and Prussian blue reaction for iron (2) and with orcein (4, 5). They are negative with von Kossa stain for calcium and the periodic acid-Schiff reaction for mucopolysaccharides (2). Based on the results of histochemical examinations and electron microscopic observations, certain substances, such as keratins produced by the odontogenic epithelium, may play a role in HB formation (2, 3, 6–8). As histochemical reactions of HBs are similar to those of dental cuticles and different from those of epithelial keratins, particular secretory proteins other than keratins have also been considered (4, 5). Alternatively, research has suggested that HBs might be derived from blood components, because HBs histochemically react to hemoglobin and iron stains. This hints at a hematogenous origin, although a histochemical reaction for hemoglobin is not specific (9, 10). Electron microscopic examination suggested that HB was formed of degenerating erythrocytes (11), not of a keratinous product of epithelial cells (11, 12). However, Browne et al. (13) disproved the possibility of both keratin and erythrocyte origin, based on the negative results of immunohistochemical staining. There have been few subsequent investigations (14, 15), and the origin of HBs is still elusive.

Our interest in the topic derives from an article by Kusama et al., (16) which showed that ectopic expression of hair keratin could be detected specifically in the ghost cells of calcifying cystic odontogenic tumor (CCOT). We confirmed the result and further found that hyaline substances in odontogenic epithelial tumors, such as odontoma and adenomatoid odontogenic tumor, were also positive for hair keratin (our unpublished observation). Considering the histological similarities between these hyaline substances in odontogenic tumors and HBs in odontogenic cysts, these observations prompted us to check the possibility that HB formation might be related to ectopic expression of

	J O P	1 1 5 0	B	Dispatch: 27.3.12	Journal: JOP	CE: Krithika P.
	Journal Name	Manuscript No.		Author Received:	No. of pages: 5	PE: Mohana L

hair keratin in the lining epithelium. In this study, we test this hypothesis, as well as the hematogenous theory, using current immunohistochemical techniques.

Materials and methods

Clinical specimens

Four hundred odontogenic cysts, including 245 radicular cysts, 146 dentigerous cysts and nine residual cysts, were screened for HBs through the archives of the Dental Hospital of Tokyo Medical and Dental University, and 10 specimens that contained HBs were obtained. Two specimens of CCOT and one specimen of skin containing hair follicles were also collected and used for controls. The experiment was approved by the university ethics committee.

Staining

Immunohistochemical staining was performed using Shandon's cassettes. For antigen retrieval, the sections were autoclaved in TE buffer (10 mM Tris (pH = 9.0) and 1 mM EDTA) at 120°C for 10 min. The primary antibodies used in this study were anti-hair keratin 1 (AE13; Santa Cruz Biotechnology, CA, USA), anti-keratin 17 (E3; Dako, Glostrup, Denmark), anti-keratin 19 (EP1580Y; Epitomics, CA, USA), and anti-hemoglobin alpha chain (EPR3608; Epitomics). The antibodies were diluted 1:500 in 50 mM Tris (pH = 7.6)/0.1% Tween 20. As a negative control, the primary antibodies were replaced by normal rabbit or mouse IgG and incubated at 4°C overnight. Envision Dual link (Dako) was used as the secondary antibody. Coloration was carried out in DAB substrate. Prussian blue staining, orcein staining, and amyloid staining were performed as previously described (17). Amyloid staining was also performed with Direct Fast Scarlet 4BS (Muto Pure Chemicals, Tokyo, Japan) replacing Congo red.

Protein extraction and Western blot analysis

Paraffin-embedded specimens were sectioned at a thickness of 10 µm and deparaffinized. Tissues were manually dissected under a microscope. The collected tissues were heated at 95°C for 1 h and then at 60°C for 4 h in extraction buffer (2.6 M thiourea, 5 M urea, 50 mM Tris-HCl (pH = 8.5), 1% CHAPS, and 5% 2-mercaptoethanol). SDS-PAGE and Western blot analyses were performed as previously described (18).

Results

We examined 10 odontogenic cysts (five radicular, four dentigerous, and one residual) with HBs, which were eosinophilic amorphous bodies that were rod-shaped or curved, or occasionally globular in the lining epithelium (Fig. 1A). Inflammation was variably observed. Hemorrhage or hemosiderin-laden macrophages were observed in all cases (Table 1). All HBs were strongly stained by orcein and Congo red (and direct fast scarlet) (Fig. 1A, Table 1). Birefringence was faintly observed. Prussian blue stain showed variable results: some HBs

were strongly stained while the others were almost negative (Table 1). We next performed immunohistochemical examination. The anti-hair keratin antibody was first submitted to validation study, which showed distinct staining localized in the hair cortex and medulla (Fig. 1B). In CCOT, ghost cells and hyaline substances were positive for hair keratin (Fig. 1C). Hair keratin was detected specifically in HBs of all the cases. The staining intensities tended to be less in the cases with extensive inflammation or hemorrhage (Table 1), suggesting that HB formation is still underway. The expression of hair keratin in the lining epithelium was faint, even in cells surrounding HBs (Fig. 1A). We also examined keratin 17 (K17), which is an epithelial keratin that is expressed in the external root sheath and medulla (Fig. 1C) and is usually absent in odontogenic cysts (19, 20). K17 was observed in HBs of all cases and also in the lining epithelium in a scattered fashion (Fig. 1A). In addition, HBs were consistently positive for hemoglobin alpha chain (Fig. 1A). To confirm the immunohistochemical observation, the tissue regions containing HBs were dissected and protein was extracted for Western blot analysis. Protein of sufficient quality and quantity was obtained from two specimens with HBs, which exhibited a single band of the expected size (Fig. 1D). Protein samples from cysts without HBs did not reveal the Western signal. Collectively, these results indicate that HBs consist of hair keratin, epithelial keratins, and hemoglobin. Notably, hair keratin, which is not usually detected in the odontogenic epithelium, was concentrated specifically in HBs.

Discussion

The restricted and consistent presence of hair keratin strongly suggests its essential role in HB genesis. HBs show a histological appearance that suggests a highly resilient nature (2), and, in fact, during tissue manipulation we found that HBs were hardly breakable. This seems consistent with the elastic property of keratin.

The development of hair and teeth is governed by similar molecular mechanisms (21), and a tendency of transdifferentiation from odontogenic to trichogenic cells may occur in tumor cells (16, 22, 23). Hair keratin production in odontogenic cysts may be understood as a similar transdifferentiation, or it may be mere dysregulation of keratin expression, as seen in certain cancer cells. Ectopic induction of truncated hair keratin (keratin 81) occurs in breast cancer cells by activation of a cryptic promoter (24, 25). Truncated hair keratin synthesis in HBs seems plausible, and this possibility should be checked in future studies because some electron microscopic observations have failed to identify keratin fibers in HBs (11, 12).

We could not find cells that were strongly positive for hair keratin in our HB samples, suggesting that the induction of hair keratin expression occurred as a localized and temporary event. As hair keratins are induced during terminal differentiation (26, 27), the cells that produced hair keratins may have already disappeared. In contrast, K17 was observed in both the HBs

COLOUR

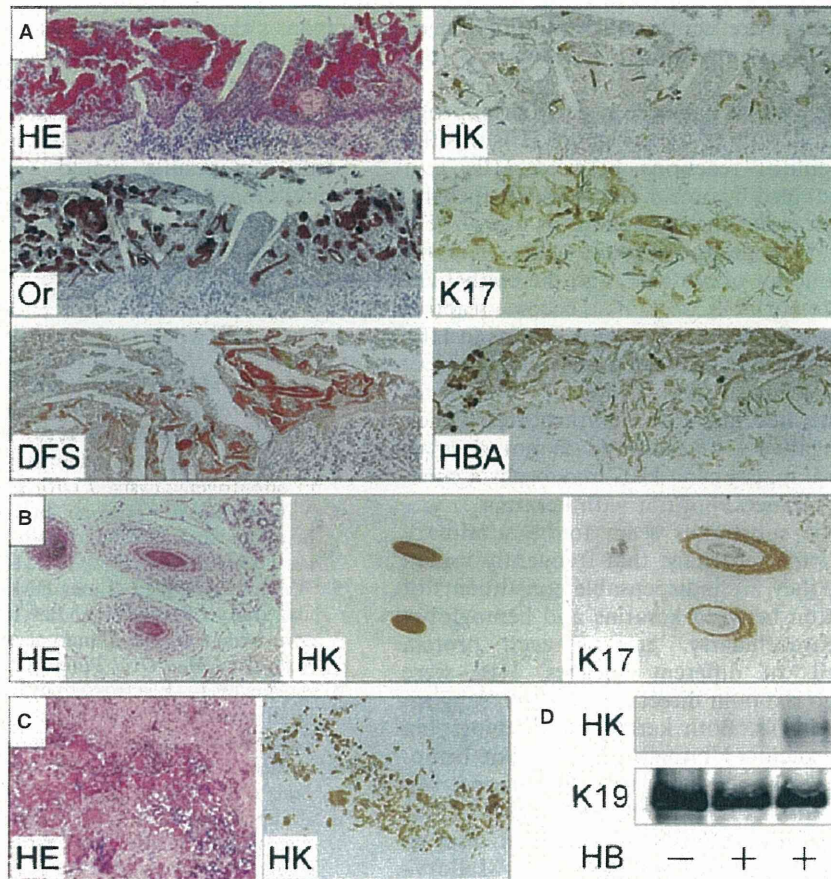


Figure 1 Keratins and hemoglobin constitute hyaline bodies. (A) Hyaline bodies in the lining epithelium of odontogenic cyst, stained with hematoxyline and eosin (HE), direct fast scarlet (DFS), anti-hair keratin (HK), anti-keratin 17 (K17), and anti-hemoglobin alpha chain (HBA) antibodies. The antigen-retrieval procedure detached some of the hyaline bodies from the glasses, causing a decrease in their numbers in immunologically stained slides (HK, K17, HBA). (B) Hair keratin and K17 expression in hairs and hair follicles. Hair keratin is expressed specifically in the medulla and cortex of hair. K17 is expressed in the external root sheath and weakly in the medulla. K17 is also expressed in the myoepithelial cells of the sweat gland. (C) Hair keratin in ghost cells and hyaline substances in calcifying cystic odontogenic tumor. (D) Western blot analysis of the protein extracted from paraffin-embedded specimens. Cysts with hyaline bodies exhibited a signal corresponding to hair keratin (HK). Keratin 19 (K19) was used as a loading control.

Table 1 Clinicopathological summaries, and histochemical and immunohistochemical results of the hyaline bodies. The site of the lesion is represented by FDI's two-digit system

Age, sex	Site	PD	Inflammation	Hemorrhage	Orcein	Congo red ^{*3}	Fe	HK	K17	HBA
29, m	11, 21	ra	++	+	+	+	+	+	+	+
42, f	21, 22	ra	+	+	+	+	-	+	+	+
43, m	21, 22	ra	++	++	+	+	+	± ^{*5}	+	+
47, m	47	ra	++	++	+	+	± ^{*4}	± ^{*5}	+	+
73, m	21	ra	± ^{*1}	+	+	+	+	+	+	+
12, f	45	de	++	+	+	+	± ^{*4}	± ^{*5}	+	+
13, m	11, 21	de	+	+	+	+	++	+	+	+
40, m	48	de	± ^{*1}	± ^{*2}	+	+	-	+	+	+
46, m	47	de	+	± ^{*2}	+	+	-	+	+	+
43, m	36	re	+	+	+	+	++	+	+	+

PD, pathological diagnosis; Fe, Prussian blue stain; HK, hair keratin; K17, keratin 17; HBA, hemoglobin alpha chain; ra, radicular cyst; de, dentigerous cyst; re, residual cyst; *1, inflammation only in the cyst wall excluding the lining epithelium; *2, no hemorrhage, but hemosiderin-laden macrophages are observed; *3, although the evaluation was carried out by direct fast scarlet staining, the title of 'Congo red' was used because it is more familiar as amyloid staining; *4, weak staining; *5, weak staining.

and the cells, which may reflect the differentiation fate of K17-expressing cells as presumptive precursors of the medulla (28, 29).

A piece of evidence that has been used to disprove the contribution of keratin to the genesis of HBs was the different histochemical reactions between HBs and keratin. HBs are stained by orcein and aldehyde fuchsin, which do not stain either the epithelium or hair. These dyes are highly reactive to sulfonic acids. Keratin contains a high amount of cysteine, and the epithelium and hair, which are normally unstained, become reactive to these dyes after oxidization (30, 31). Keratins in HBs may not be at normal biochemical conditions, but may have been highly oxidized. As we noticed that orcein stained the degenerated and fused erythrocytes, which were virtually negative for keratin (data not shown), these histochemical reactions in HBs may occur against hematogenous substances, but not with keratins.

The erythrocytic substances seem to be subsidiary deposits because of hemorrhage that frequently occurs in jaw cysts; still, they are indispensable constituents of HB. The interaction between keratins and hemoglobin would occur extracellularly, because each protein derives from cells of different lineages. HBs were positive for Congo red (and direct fast scarlet), suggesting cross β -sheet fibrils. Both keratin and hemoglobin are α -helix-rich proteins. However, extracellular hemoglobin can convert from α -helix to β -sheet, especially under acidic conditions (32). Keratins K8 and K18 also convert to cross β -sheet in hepatocytes of liver diseases (33) and aggregate to form inclusions called Mallory-Denk bodies (34, 35). This conversion is an intracellular event, but the keratins also spontaneously change their conformations *in vitro* when extracted (33). As for the reason why the hair keratin among other keratins is required for HB formation, we think that the ectopic hair keratin may fail to arrange into filaments because of the absence of the binding partners. Once keratin fibers are formed, they are very stable, but a monomeric keratin would be susceptible to conformational change. Collectively, we assume that keratins and hemoglobin are released from dead epithelial cells and erythrocytes, respectively, undergo β -sheet conversion during degeneration, and aggregate to form HBs. Abundance of both proteins would permit swift formation of HBs, which is crucial to be histologically recognized, because they will eventually move out into the cystic space by turnover of the lining epithelium. Although HB is not a pathogenic amyloid as seen in protein conformation diseases, our results would add novel keratins and hemoglobin to the list of amyloidogenic proteins. Recently, orcein has been shown to strongly bind to protofibrils of amyloid- β precursor protein (36). If such is the case, the above-mentioned orcein reactivity to degenerated erythrocytes may suggest proamyloid formation by hemoglobin prior to keratin aggregation.

In conclusion, the present study demonstrates that HBs are amyloids that are formed as a consequence of two independent biological events: unusual alteration of epithelial differentiation so as to provide hair keratin, and hemorrhage so as to provide hemoglobin. Although

emphasis should be placed on the ectopic production of hair keratins, our results reconcile the long-standing debate between two theories, the keratin theory versus the hematogenous theory, concluding that both substances are required for the genesis of HBs. Furthermore, our results would add novel keratins and hemoglobin to the list of non-pathological amyloidogenic proteins.

References

1. Dewy KW. Cysts of the dental system. *Dent Cos* 1918; **60**: 555.
2. Rushton MA. Hyaline bodies in the epithelium of dental cysts. *Proc R Soc Med* 1955; **48**: 407-9.
3. Morgan PR, Johnson NW. Histological, histochemical and ultrastructural studies on the nature of hyalin bodies in odontogenic cysts. *J Oral Pathol* 1974; **3**: 127-47.
4. Yamaguchi A. Hyaline bodies of odontogenic cysts: histological, histochemical and electron microscopic studies. *J Oral Pathol* 1980; **9**: 221-34.
5. Wertheimer FW, Fullmer HM, Hansen LS. A histochemical study of hyaline bodies in odontogenic cysts and a comparison to the human secondary dental cuticle. *Oral Surg Oral Med Oral Pathol* 1962; **15**: 1466-73.
6. Allison RT. Electron microscopic study of 'Rushton' hyaline bodies in cyst linings. *Br Dent J* 1974; **137**: 102-4.
7. Zegarelli DJ, Zegarelli-Schmidt EC, Zegarelli EV. Hyaline bodies: some observations on their ultrastructure. *Oral Surg Oral Med Oral Pathol* 1976; **42**: 643-53.
8. Philippou S, Ruhl GH, Mandelartz E. Scanning electron microscopic studies and x-ray microanalysis of hyaline bodies in odontogenic cysts. *J Oral Pathol Med* 1990; **19**: 447-52.
9. Dent RJ, Wertheimer FW. Hyaline bodies in odontogenic cysts: a histochemical study for hemoglobin. *J Dent Res* 1967; **46**: 629.
10. Sedano HO, Gorlin RJ. Hyaline bodies of Rushton. Some histochemical considerations concerning their etiology. *Oral Surg Oral Med Oral Pathol* 1968; **26**: 198-201.
11. El-Labban NG. Electron microscopic investigation of hyaline bodies in odontogenic cysts. *J Oral Pathol* 1979; **8**: 81-93.
12. Jensen JL, Erickson JO. Hyaline bodies in odontogenic cysts: electron microscopic observations. *J Oral Pathol* 1974; **3**: 1-6.
13. Browne RM, Matthews JB. Intra-epithelial hyaline bodies in odontogenic cysts: an immunoperoxidase study. *J Oral Pathol* 1985; **14**: 422-8.
14. Fujita S, Takahashi H, Okabe H. Immunohistochemical and ultrastructural study of hyaline bodies in odontogenic cysts. *Shika Kiso Igakkai Zasshi* 1989; **31**: 211-7.
15. Pesce C, Ferloni M. Apoptosis and Rushton body formation. *Histopathology* 2002; **40**: 109-11.
16. Kusama K, Katayama Y, Oba K, et al. Expression of hard alpha-keratins in pilomatrixoma, craniopharyngioma, and calcifying odontogenic cyst. *Am J Clin Pathol* 2005; **123**: 376-81.
17. Bancroft JD, Gamble M. *Theory and practice of histological techniques*. Xxxxxxxx: Elsevier Health Sciences, 2008. **3**
18. Taylor GP. *Current protocols in molecular biology*. Xxxx: Wiley, 1987. **4**
19. Aragaki T, Michi Y, Katsube K, et al. Comprehensive keratin profiling reveals different histopathogenesis of keratocystic odontogenic tumor and orthokeratinized odontogenic cyst. *Hum Pathol* 2010; **41**: 1718-25.

20. Tsuneki M, Yamazaki M, Cheng J, et al. Combined immunohistochemistry for the differential diagnosis of cystic jaw lesions: its practical use in surgical pathology. *Histopathology* 2010; **57**: 806–13.
21. Thesleff I, Vaahtokari A, Partanen AM. Regulation of organogenesis. Common molecular mechanisms regulating the development of teeth and other organs. *Int J Dev Biol* 1995; **39**: 35–50.
22. Tanaka A, Okamoto M, Yoshizawa D, et al. Presence of ghost cells and the Wnt signaling pathway in odontomas. *J Oral Pathol Med* 2007; **36**: 400–4.
23. Kikuchi K, Ishige T, Fuchinoue F, et al. Expression of hard α -keratins in adenomatoid odontogenic tumor: a case study with immunohistochemical analysis. *Oral Med Path* 2008; **13**: 7–14.
24. Regnier CH, Boulay A, Asch PH, et al. Expression of a truncated form of hHb1 hair keratin in human breast carcinomas. *Br J Cancer* 1998; **78**: 1640–4.
25. Boulay A, Regnier CH, Anglard P, et al. Transcription regulation and protein subcellular localization of the truncated basic hair keratin hHb1-DeltaN in human breast cancer cells. *J Biol Chem* 2001; **276**: 22954–64.
26. Langbein L, Rogers MA, Winter H, et al. The catalog of human hair keratins. I. Expression of the nine type I members in the hair follicle. *J Biol Chem* 1999; **274**: 19874–84.
27. Langbein L, Rogers MA, Winter H, et al. The catalog of human hair keratins. II. Expression of the six type II members in the hair follicle and the combined catalog of human type I and II keratins. *J Biol Chem* 2001; **276**: 35123–32.
28. McGowan KM, Coulombe PA. Keratin 17 expression in the hard epithelial context of the hair and nail, and its relevance for the pachyonychia congenita phenotype. *J Invest Dermatol* 2000; **114**: 1101–7.
29. Langbein L, Yoshida H, Praetzel-Wunder S, et al. The keratins of the human beard hair medulla: the riddle in the middle. *J Invest Dermatol* 2010; **130**: 55–73.
30. Lillie RD, Bangle R, Fisher ER. Metachromatic basophilia of keratin after oxidation-cleavage of disulfide bond. *J Histochem Cytochem* 1954; **2**: 95–102.
31. Fullmer HM, Lillie RD. Some aspects of the mechanism of orcein staining. *J Histochem Cytochem* 1956; **4**: 64–8.
32. Mahato M, Pal P, Kamilya T, et al. pH induced structural modulation and interfacial activity of hemoglobin at the air/water interface. *J Phys Chem B* 2010; **114**: 495–502.
33. Mahajan V, Klingstedt T, Simon R, et al. Cross beta-sheet conformation of keratin 8 is a specific feature of Mallory-Denk bodies compared with other hepatocyte inclusions. *Gastroenterology* 2011; **141**: 1080–90 e1–7.
34. Zatloukal K, French SW, Stumptner C, et al. From Mallory to Mallory-Denk bodies: what, how and why? *Exp Cell Res* 2007; **313**: 2033–49.
35. Hazan R, Denk H, Franke WW, et al. Change of cytokeratin organization during development of Mallory bodies as revealed by a monoclonal antibody. *Lab Invest* 1986; **54**: 543–53.
36. Bieschke J, Herbst M, Wiglenda T, et al. Small-molecule conversion of toxic oligomers to nontoxic beta-sheet-rich amyloid fibrils. *Nat Chem Biol* 2012; **8**: 93–101.

Acknowledgments

This work was supported by a Grant-in-Aid for Scientific Research (C) (No. 21592320).

Author Query Form

Journal: JOP

Article: 1150

Dear Author,

During the copy-editing of your paper, the following queries arose. Please respond to these by marking up your proofs with the necessary changes/additions. Please write your answers on the query sheet if there is insufficient space on the page proofs. Please write clearly and follow the conventions shown on the attached corrections sheet. If returning the proof by fax do not write too close to the paper's edge. Please remember that illegible mark-ups may delay publication.

Many thanks for your assistance.

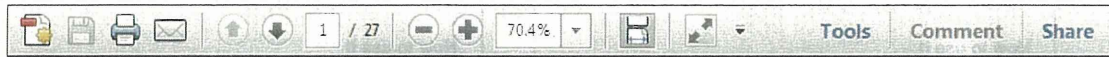
Query reference	Query	Remarks
1	AUTHOR: Please give address information for Santa Cruz Biotechnology, Epitomics: town.	
2	AUTHOR: Please check and confirm the edits made in the following sentence "As a negative control ... at 4 °C overnight."	
3	AUTHOR: Please provide the city location of publisher for reference [17].	
4	AUTHOR: Please provide the city location of publisher for reference [18].	

USING e-ANNOTATION TOOLS FOR ELECTRONIC PROOF CORRECTION

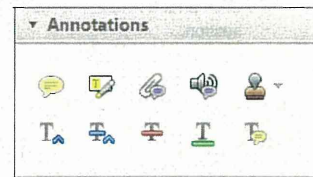
Required software to e-annotate PDFs: **Adobe Acrobat Professional** or **Adobe Reader** (version 8.0 or above). (Note that this document uses screenshots from **Adobe Reader X**)

The latest version of Acrobat Reader can be downloaded for free at: <http://get.adobe.com/reader/>

Once you have Acrobat Reader open on your computer, click on the **Comment** tab at the right of the toolbar:



This will open up a panel down the right side of the document. The majority of tools you will use for annotating your proof will be in the **Annotations** section, pictured opposite. We've picked out some of these tools below:



1. Replace (Ins) Tool – for replacing text.

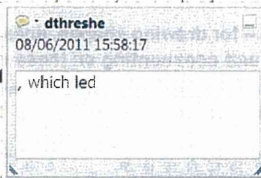


Strikes a line through text and opens up a text box where replacement text can be entered.

How to use it

- Highlight a word or sentence.
- Click on the **Replace (Ins)** icon in the Annotations section.
- Type the replacement text into the blue box that appears.

rdard framework for the analysis of m
icy. Nevertheless, it also led to exoge
ole of strateg
ber of comp
is that the st
main compo
level, are exc
important work
M henceforth we open the black b



2. Strikethrough (Del) Tool – for deleting text.



Strikes a red line through text that is to be deleted.

How to use it

- Highlight a word or sentence.
- Click on the **Strikethrough (Del)** icon in the Annotations section.

there is no room for extra profits at
cups are zero and the number of
(et) values are not determined by
Blanchard and Kiyotaki (1987).
effect competition in general equilil
ts of aggregate demand and supply
lassical framework assuming monoj
een an exogenous number of firms

3. Add note to text Tool – for highlighting a section to be changed to bold or italic.



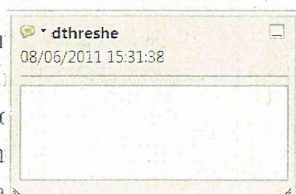
Highlights text in yellow and opens up a text box where comments can be entered.

How to use it

- Highlight the relevant section of text.
- Click on the **Add note to text** icon in the Annotations section.
- Type instruction on what should be changed regarding the text into the yellow box that appears.

dynamic responses of mark ups
ent with the **VAR** evidence

sation
y Ma
and
on n
to a
erent also with the demand.



4. Add sticky note Tool – for making notes at specific points in the text.



Marks a point in the proof where a comment needs to be highlighted.

How to use it


- Click on the **Add sticky note** icon in the Annotations section.
- Click at the point in the proof where the comment should be inserted.
- Type the comment into the yellow box that appears.

and supply shocks. Most of
a
number
dard fr
cy. Nev
ole of st
iber of competitors and the imp
is that the structure of the secto



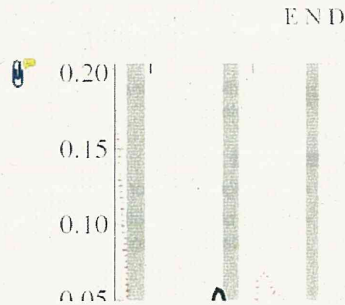
USING e-ANNOTATION TOOLS FOR ELECTRONIC PROOF CORRECTION

5. Attach File Tool – for inserting large amounts of text or replacement figures.


 Inserts an icon linking to the attached file in the appropriate place in the text.

How to use it

- Click on the **Attach File** icon in the Annotations section.
- Click on the proof to where you'd like the attached file to be linked.
- Select the file to be attached from your computer or network.
- Select the colour and type of icon that will appear in the proof. Click OK.



6. Add stamp Tool – for approving a proof if no corrections are required.

 Inserts a selected stamp onto an appropriate place in the proof.

How to use it

- Click on the **Add stamp** icon in the Annotations section.
- Select the stamp you want to use. (The **Approved** stamp is usually available directly in the menu that appears).
- Click on the proof where you'd like the stamp to appear. (Where a proof is to be approved as it is, this would normally be on the first page).

of the business cycle, starting with the
 on perfect competition, constant ret
 production. In this environment, firms
 extra
 h
 returned by the model. The New Key
 otaki (1987), has introduced produc
 general equilibrium models with nomin
 and

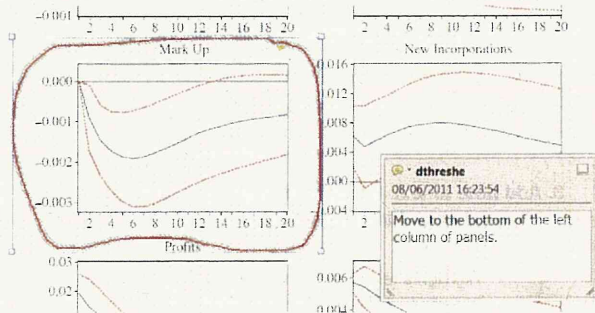



7. Drawing Markups Tools – for drawing shapes, lines and freeform annotations on proofs and commenting on these marks.

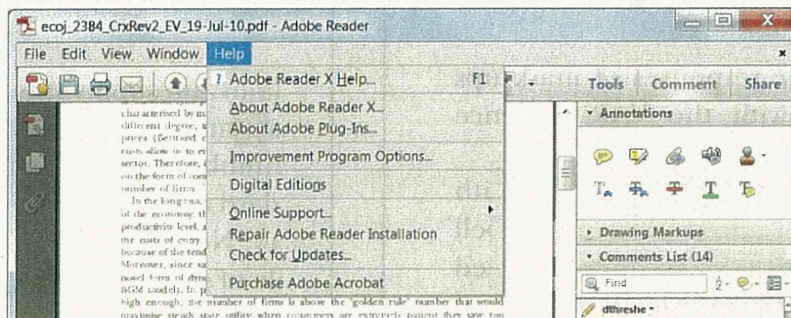
Allows shapes, lines and freeform annotations to be drawn on proofs and for comment to be made on these marks..

How to use it

- Click on one of the shapes in the **Drawing Markups** section.
- Click on the proof at the relevant point and draw the selected shape with the cursor.
- To add a comment to the drawn shape, move the cursor over the shape until an arrowhead appears.
- Double click on the shape and type any text in the red box that appears.



For further information on how to annotate proofs, click on the **Help** menu to reveal a list of further options:



Exploitation of a novel polysaccharide nanogel cross-linking membrane for guided bone regeneration (GBR)

Takayuki Miyahara^{1,4*}, Myat Nyan^{1,4}, Asako Shimoda^{2,4}, Yuka Yamamoto², Shinji Kuroda¹, Makoto Shiota¹, Kazunari Akiyoshi^{2,3,4} and Shohei Kasugai^{1,4}

¹Oral Implantology and Regenerative Dental Medicine, Tokyo Medical and Dental University, Japan

²Organic Biomaterials Institute of Biomaterials and Bioengineering, Tokyo Medical and Dental University, Japan

³Department of Polymer Chemistry, Graduate School of Engineering, Kyoto University, Japan

⁴Global Centre of Excellence (GCOE) Programme, International Research Centre for Molecular Science in Tooth and Bone Diseases, Tokyo Medical and Dental University, Japan

Abstract

Cholesterol-bearing pullulan (CHP) nanogel is a synthetic degradable biomaterial for drug delivery with high biocompatibility. Guided bone regeneration (GBR) is a bone augmentation technique in which a membrane is used to create and keep a secluded regenerative space. The purpose of the present study was to evaluate the effects of the novel CHP nanogel membrane in GBR. Thirty-six adult Wistar rats were used and bilaterally symmetrical full-thickness parietal bone defects of 5 mm diameter were created with a bone trephine burr. Each defect was covered with the collagen membrane or the CHP nanogel membrane or untreated without any membrane. The animals were sacrificed at 2, 4 and 8 weeks and analysed radiologically and histologically. Furthermore, after incubating human serum with CHP nanogel or collagen, the amount of PDGF in the serum was measured using ELISA. New bone formation in terms of bone volume was higher in the nanogel group than in the control or collagen groups at 2 and 4 weeks. At 8 weeks, both membrane groups showed higher bone volumes than the control group. Notably, the newly-formed bone in the bone defect in the nanogel group was uniform and histologically indistinguishable from the original bone, whereas in the collagen group the new bone showed an irregular structure that was completely different from the original bone. After incubating with CHP nanogel, the amount of PDGF in the serum decreased significantly. CHP nanogel GBR membrane favourably stimulated bone regeneration, in which a unique characteristic of CHP nanogel, the storage of endogenous growth factors, was likely implicated. Copyright © 2011 John Wiley & Sons, Ltd.

Received 8 February 2011; Revised 14 June 2011; Accepted 5 July 2011

Keywords guided bone regeneration; biomaterials; bone regeneration; acryloyl group-modified cholesterol-bearing pullulan (CHPOA); morphometric analysis; radiology; membrane; animal experiments

1. Introduction

Dental rehabilitation of totally or partially edentulous patients with dental implants has become a routine treatment modality in recent decades, with reliable long-term

results (Albrektsson *et al.*, 1981, 1986; van Steenberghe, 1989; van Steenberghe *et al.*, 1990; Lindquist *et al.*, 1996; Buser *et al.*, 1997; Arvidson *et al.*, 1998; Lekholm *et al.*, 1999; Brocard *et al.*, 2000; Leonhardt *et al.*, 2002). However, local conditions of the alveolar ridge, bone volume and bone quality, affect the long-term prognosis. Guided tissue regeneration (GTR) (Nyman *et al.*, 1982, 1990) was originally developed for the treatment of periodontal defects and then the same concept was later applied to bone regeneration, which is called guided bone regeneration (GBR) (Dahlin *et al.*, 1989). Vertical and horizontal bone augmentation with GBR has been

* Correspondence to: T. Miyahara, Oral Implantology and Regenerative Dental Medicine, Tokyo Medical and Dental University, 1-5-45 Yushima, Bunkyo-ku, Tokyo 113-8549, Japan. E-mail: miyahara.irm@tmd.ac.jp

applied to improve alveolar ridge deformities (Buser *et al.*, 1993; Simion *et al.*, 1996; Urban *et al.*, 2009). In GBR procedures, the barrier membrane keeps the bone regeneration space and it also prevents the invasion of fibrous connective tissue, resulting in new bone formation under the membrane.

Several different membranes, including non-resorbable and resorbable membranes, have been developed and clinically used in GBR. Resorbable membranes have been generally preferred because the second surgery for its removal was unnecessary, rendering the procedure less invasive to patients. Biomaterials such as collagen or copolylactic/glycolic acid (PLGA) have been developed as degradable GBR membranes. Since collagen is an animal-derived material, the risk of unknown infection is undeniable and an unfavourable immune response occurs in some patients (Charriere *et al.*, 1989; Keefe *et al.*, 1992; Lynn *et al.*, 2004).

Although PLGA is a completely synthetic material, it will gradually produce acids, inducing inflammatory responses. These disadvantages are not clearly noticed clinically; however, developing more biocompatible synthetic GBR membrane is beneficial.

Hydrophobized polysaccharide, such as cholesterol-bearing pullulan (CHP), is a unique material for drug delivery systems (DDSs) (Akiyoshi *et al.*, 1998, 1999, 2002, Akiyoshi, 2006). Cholesterol-bearing pullulan (CHP) self-aggregates to form a monodisperse and stable hydrogel nanoparticle, in which the domains of the associated cholesterol groups of CHP provide cross-linking points in a non-covalent manner (Figure 1). The size and density of the hydrogel nanoparticle can be controlled by changing the degree of substitution of the cholesterol groups of CHP. During that substitution process, it can incorporate growth factors and act as a molecular chaperone. We have reported that delivering prostaglandin E1 with CHP nanogel stimulates wound healing in rats (Kobayashi *et al.*, 2009). In this previous study it was surprising to find that CHP nanogel alone enhanced wound healing. Therefore, the barrier membrane containing CHP nanogel may have great potential as a GBR membrane. The purpose of the present study was to evaluate the effectiveness of the novel bioabsorbable CHP nanogel cross-linking membrane as a GBR membrane.

2. Materials and methods

2.1. Collagen membrane

A bioabsorbable membrane made of collagen (Koken Tissue Guide[®], Japan) was used. This material was combined with bovine collagen derived from dermis tissue and bovine insoluble collagen derived from tendon (9:1). It was freeze-dried and cross-linked with the addition of hexamethylenediisocyanate (HMDIC). The collagen membranes were cut into circles with a diameter of approximately 6 mm.

2.2. Nanogel cross-linking membrane

CHP was synthesized as reported previously (Akiyoshi *et al.*, 1996). Acryloyl group-modified cholesterol-bearing pullulan (CHPOA) nanogel was synthesized by the reaction of 2-(acryloyloxy)-ethyl isocyanate (AOI) and CHP. CHPOA nanogel solution (40.5 μ l, 26.7 mg/ml) in Dulbecco's phosphate-buffered saline (PBS; pH 7.4) and 5.4 μ l DMSO were mixed and kept at 4 °C for 24 h. This CHPOA nanogel solution and 8.1 μ l solution of PEG-SH in PBS (481.8 mg/ml) were mixed at the ratio of thiol groups to acryloyl groups, which was 1:1. Then 13 μ l of the mixture was placed between two glass slides coated with Parafilm[®] for 4 h at 37 °C under humidified conditions, to form a membrane-shaped hydrogel. The diameter and thickness of the nanogel membrane was 6 and 0.4 mm, respectively. The prepared membrane was applied to bone defects of experimental animals within 24 h.

2.3. Animal experiments

The animal experiments in the present study were approved by the Committee of Animal Experiments, Tokyo Medical and Dental University.

2.4. Surgical procedures

Thirty-six adult male Wistar rats, 16 weeks old, were used and divided into three groups. Prior to the experiment, the overall health of each rat was monitored for 2 weeks. The rats were kept in a standard cage (Tokiwai, Japan) in an experimental animal room at 22 \pm 3 °C at 40–60% humidity and 1 atm, on 6:00–20:00 light, fed a standard laboratory diet (CE-2 CLEA Japan Inc.) and given sterilized water. The animals were anaesthetized with a combination of ketamine (40 mg/kg)–xylazine (5 mg/kg). In addition, approximately 0.4 ml local anaesthesia with lidocaine–HCl containing epinephrine 1/80 000 (2% Xylocain, Astra Japan Ltd, Fujisawa Pharmaceutical Co. Ltd, Osaka, Japan) was injected at the surgical site. A cutaneous flap was created by making a mid-sagittal incision through the skin, which was raised from the forehead. The periosteum was incised and elevated to expose the calvarial bone on both sides of the midline. Two symmetrical, full-thickness bone defects with outer diameter of 5 mm were created with a bone trephine burr (Tele Components Co., Germany) under continuous saline irrigation. The defects were covered with CHP nanogel cross-linking membrane or collagen membrane or without any membrane. The animals were sacrificed under chloroform anaesthesia at 2, 4 and 8 weeks after the surgery and analysed radiologically and histologically.

2.6. Radiographic evaluation

The calvariae were dissected out and fixed in neutral 10% formalin and then analysed using micro-CT (μ CT; InspeXio, Shimadzu Science East Corp., Tokyo, Japan) to measure the bone volume in the defect area.

Novel nanogel cross-linking membrane for GBR

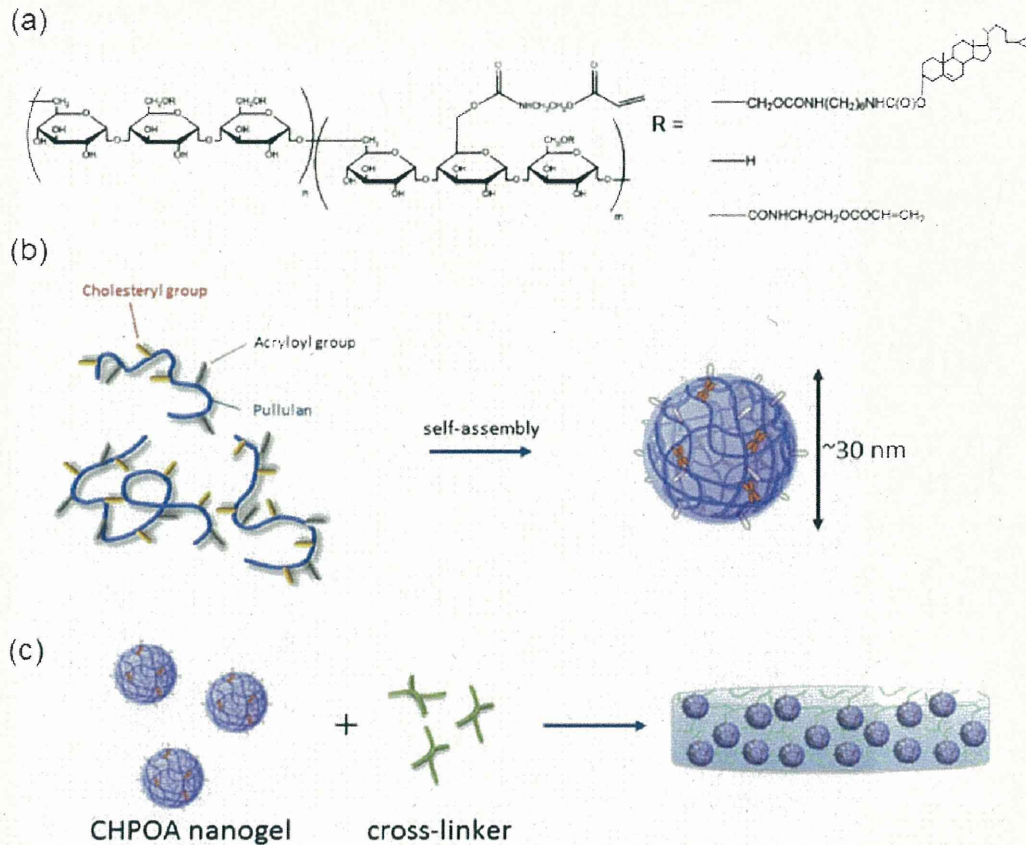


Figure 1. Scheme of acryloyl group-modified cholesterol-bearing pullulan (CHPOA). (A) Chemical structure of CHPOA nanogel. (B) Schematic illustration of CHPOA. (C) Schematic illustration of CHPOA nanogel cross-linking hydrogel (CHPOA-PEGSH)

2.7. Histological analysis

After radiographic analysis the calvariae were decalcified in 5% formic acid for 2 weeks. The specimens were dehydrated in ascending grades of ethanol, embedded in paraffin and sectioned 5 μm thick in the sagittal direction with a microtome. The sections were stained with haematoxylin and eosin (H&E).

2.8. PDGF concentration after incubating serum with materials, ELISA

Whole blood (50 ml) was obtained from the arm vein of a healthy, non-smoker male donor aged 34 years. After being stored overnight in a glass tube at room temperature, serum was prepared. The serum was incubated in three different combinations: serum alone, serum with collagen membrane and serum with nanogel membrane. The diameter of both membranes was 6 mm. These combinations were prepared in Eppendorf-type 1.5 ml vials and incubated for 3 h at room temperature. Then, PDGF-BB concentration in the serum was measured using an ELISA kit (Human PDGF-BB ELISA Kit, Ray Bio[®], Ray Biotech Inc., Norcross, GA, USA) according to the manufacturer's instructions.

2.9. Statistical analysis

Data, apart from the ELISA result, were first analysed by one-way ANOVA. When this analysis suggested a significant difference between groups, the data were further analysed by Tukey *post hoc* multiple comparison tests, using SPSS software (v 11.5, SPSS, Chicago, IL, USA). For ELISA assay, statistical evaluation was performed with Student's *t*-tests (SPSS v 11.5). $p < 0.05$ was considered to be statistically significant.

3. Results

3.1. Radiographical images

Post-operative soft tissue healing was similar in all three groups without any membrane exposure in both membrane groups. The radiographical images of all the groups at 2, 4, and 8 weeks are presented in Figure 2. In the control group, newly formed bone could be seen only at the surrounding edge of the defect. In the collagen membrane group, part of the membrane appeared to be calcified, whereas in the CHP nanogel membrane group newly formed bone could be observed in almost the entire defected area. The surface of new bone in the CHP

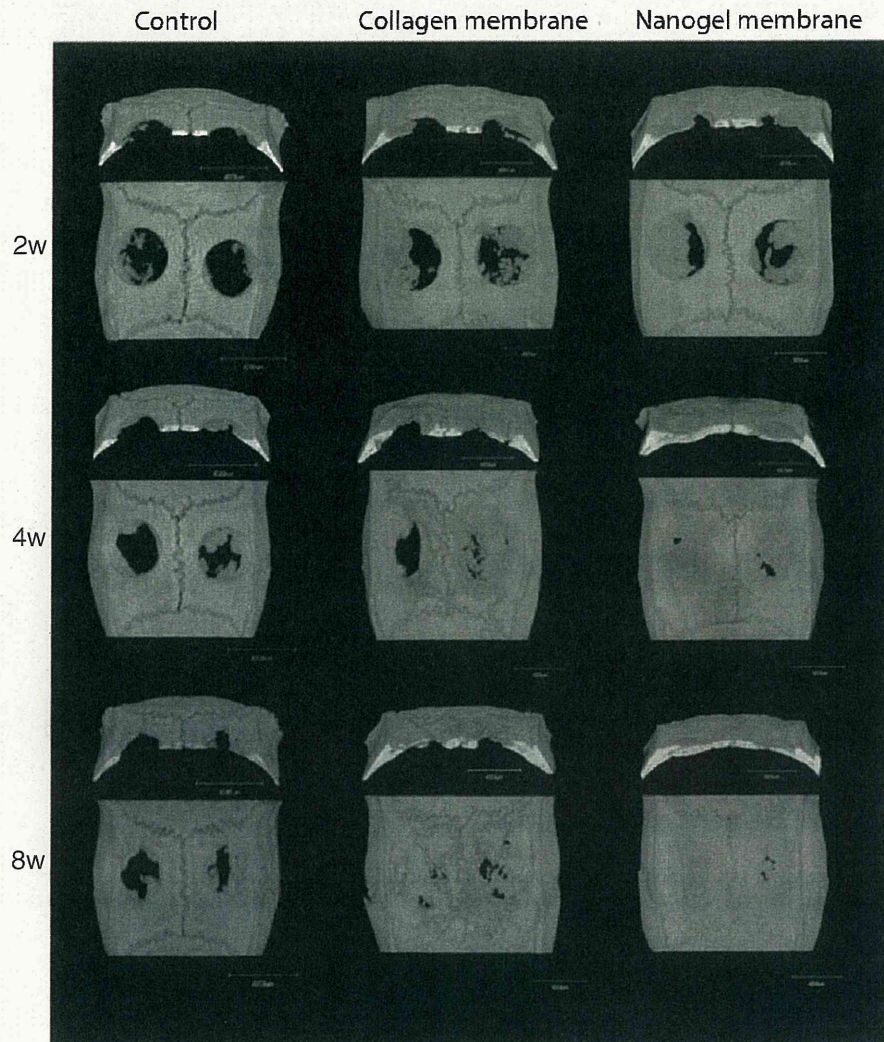


Figure 2. Cross-sectional micro-CT images of the bone defects at 2, 4 and 8 weeks

nanogel group was smooth; however, that in the collagen group was irregular. Volume of the newly formed bone is shown in Figure 3. New bone volume in the defect area in CHP nanogel group was highest at 2 and 4 weeks. At 8 weeks there was no statistical difference of newly-formed bone volume between the collagen and CHP nanogel groups. Newly-formed bone volume in the control group was lowest at the three time points.

3.2. Histological images

Histological images are presented in Figure 4. Corresponding to the radiographical images, new bone formation in CHP nanogel was prominent at 2 and 4 weeks compared with the other two groups. Notably, newly-formed bone in the CHP nanogel group was mature bone containing less connective tissue (Figure 4c, f, i, l),

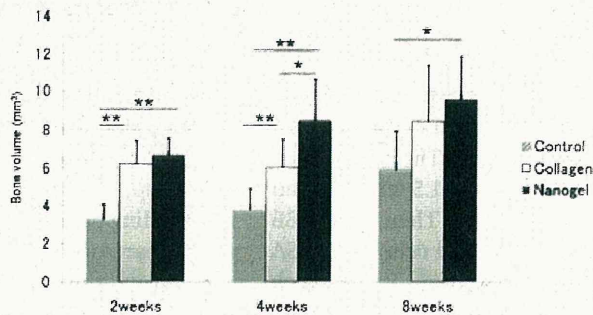


Figure 3. Bone volume in the defects at 2, 4 and 8 weeks. The data were obtained with micro-CT analysis. * $p < 0.05$, ** $p < 0.01$

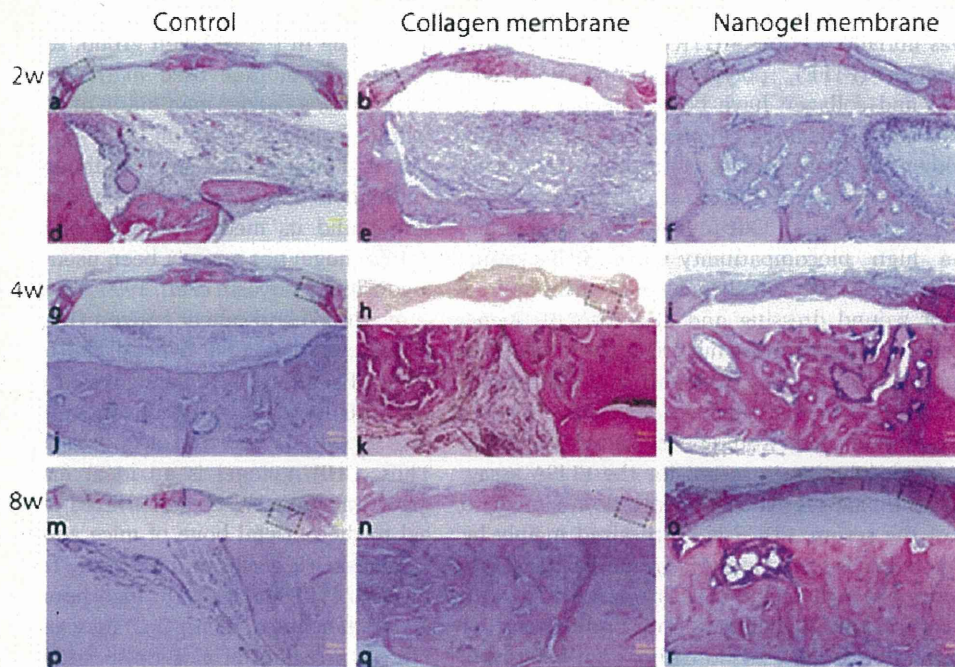


Figure 4. Histological images at 2, 4 and 8 weeks. High-magnification images of the parts of low-magnified images are presented; H&E staining

whereas in the collagen group less mature irregular bone was observed (Figure 4b, e, h, k). In addition, in the CHP nanogel group new bone formation occurred under the membrane, while it was observed both inside and under the membrane in the collagen group.

3.3. PDGF concentration after incubating serum with materials, ELISA

After incubating serum with the membranes, PDGF-BB concentration in the serum was measured. PDGF-BB concentration in the serum was the lowest when the serum was incubated with CHP nanogel membrane (Table 1), suggesting that CHP nanogel membrane trapped PDGF-BB in the material.

4. Discussion

The principle of GBR was originally explored for bone augmentation of the alveolar process in conjunction with

Table 1. PDGF concentration in the serum after incubating with collagen membrane or CHP nanogel membrane

	Mean \pm SD (pg/ml)
Serum	164.0 \pm 5.0
Serum + collagen	163.3 \pm 4.7
Serum + nanogel	151.9 \pm 6.7

* $p < 0.05$, significantly different from one another.

oral implant therapy (Dahlin *et al.*, 1988; Buser *et al.*, 1993; Simion *et al.*, 1996; Urban *et al.*, 2009). In GTR and GBR, a membrane is used to keep regenerative space, preventing the invasion of the unfavourable surrounding tissue. The concept of tissue engineering is to provide the three key players to the regenerative site: cells, signal molecules and scaffolds; it is obvious that in both GTR and GBR, cells, signal molecules and scaffolds are endogenous. The progenitor cells are derived from the tissue facing the regenerative site, not from the tissue separated by a membrane. Signal molecules from activated platelets, such as PDGF and TGF- β , initially work for proliferation and differentiation of osteogenic cells. As scaffolds, fibrin initially plays important roles in regeneration. Collagen and other extracellular matrices are produced by the cells in the regenerative space and they work as scaffolds. Thus, GTR and GBR are characterized as encouraging endogenous regenerative ability by providing a space for regeneration.

In the present study, a bone defect model of rat calvaria was used to evaluate two types of GBR membrane. Although bone regeneration in the internal bone defect is different from external bone augmentation in GBR, the potential of the material for GBR membrane could be evaluated in the internal bone defect model of the present study. The present bone defect of 5 mm diameter did not heal spontaneously at 8 weeks when the defect was left without a membrane. The proliferation of undesired soft tissues in the bone defect interrupts the proliferation of bone forming cells from the periphery of the defect (Dahlin *et al.*, 1988; Kostopoulos *et al.*, 1994; Hämmerle *et al.*, 1995). Any material with some degree of biocompatibility can work as GTR or GBR membrane. Methyl

cellulose was initially used as a GTR membrane. Polytetrafluoroethylene (PTFE), polyglycolic and polylactic acids (PLGA) and collagen have been clinically applied as GBR membranes (Bunyaratavej and Wang, 2001). Furthermore, other materials, such as chitin/chitosan and alginate, have also been investigated as GBR membranes (Eun-Jung Lee *et al.*, 2009). Our previous studies demonstrated the high biocompatibility of CHP nanogel (Kobayashi *et al.*, 2009), which is one of the required properties for wound dressing and also for GBR membranes. Compared with the other materials, the uniqueness of CHP nanogel is to trap hydrophobic and hydrophilic molecules inside. Since CHP nanogel contains > 90% of water, the water in the gels would be exchanged for tissue exudates. After incubating in serum for the ELISA assay, the colour of the nanogel changed into yellow, similar to the colour of the serum. PDGF is synthesized mainly by megakaryocytes and is stored in the α -granules of platelets. When platelets are activated, PDGF is released. *In vitro*, PDGF-AA and PDGF-BB enhance the proliferation of multiple types of bone cells, including both osteoblast and osteoclast lineages (Hadjidakis and Androulakis, 2006; Zhang *et al.*, 1998). Although long-term exposure to PDGF reduces alkaline phosphatase activity and mineralization (Hsieh and Graves, 1998), application of PDGF stimulates regeneration of periodontal tissue and bone (Nevens *et al.*, 2009).

In our previous study, CHP nanogel alone stimulated wound healing in rats (Kobayashi *et al.*, 2009) and we speculated that CHP nanogel stored endogenous growth factors in wound exudates. In the present study, the decrease in the amount of PDGF-BB in the serum was small but significant after incubating the serum with CHP nanogel membrane. The result of the ELISA assay indicated that CHP nanogel membrane has an ability to store PDGF-BB. It is also possible that CHP nanogel membrane would store not only PDGF-BB but also other growth factors produced at the regenerative site. In addition to PDGF-BB, TGF- β , VEGF and FGF are also produced in and around the bone defects. It is likely that after storing growth factors at the regenerative site, CHP nanogel membrane would gradually release these growth factors during membrane degradation; in other words, it is reasonable to conclude that CHP nanogel membrane works as signal molecule attractant and reservoir at the regenerative site.

In the present study, both collagen and CHP nanogel membrane stimulated bone regeneration compared to the control, in which no membrane was applied. The amount of newly-formed bone at the early time point and the quality of the bone in the CHP nanogel group were superior to that of the collagen group. The character of the CHP nanogel membrane, storing and releasing endogenous growth factors, could partly explain this difference. In the histological images, bone was formed under the membrane in the CHP nanogel group, whereas it was formed both inside and under the membrane in the collagen group. In the μ CT images we also observed the irregular surface of the regenerated bone facing the

membrane in the collagen group. It is plausible that the collagen membrane used in the present study worked not only as a barrier membrane of GBR but also as a scaffold for bone regeneration.

CHP nanogel consists of pullulan and cholestesterol. Pullulan is a polysaccharide industrially prepared from starch and its medical application has been approved. CHP nanogel has already been used clinically for delivering insulin (Akiyoshi *et al.*, 1998), interleukin 12 (Shimizu *et al.*, 2008) and cancer antigen (Kageyama *et al.*, 2008); in these studies, CHP nanogel did not exert any adverse effect. Therefore, CHP nanogel is an extremely safe material. The uniqueness of CHP nanogel is that it can incorporate growth factors and acts as a molecular chaperone. Thus, CHP nanogel is an ideal material for delivering growth factors. We have delivered BMP2 with CHP nanogel to the parietal bone of mice and observed new bone formation (Hayashi *et al.*, 2009). In addition to growth factors, CHP nanogel can incorporate small biologically active molecules. Using CHP nanogel we have also delivered prostaglandin E agonist and prostaglandin E1 to bone and skin wounds, respectively, and reported the stimulation of bone and skin regeneration (Kobayashi *et al.*, 2009; Kamolratanakul *et al.*, 2011). The present study demonstrated that CHP nanogel membrane alone stimulated bone regeneration; however, delivering biologically active molecules, such as BMP and prostaglandin E1, with CHP nanogel would be effective and promising in bone regeneration (Hayashi *et al.*, 2009). Although CHP nanogel membrane is promising as a GBR membrane, we have to solve the following two points before applying this membrane in GBR clinically. First, the membrane should be stable for a long time at room temperature. In the present study, CHP nanogel membrane was prepared within 24 h before the surgical application. It would be possible to make CHP nanogel membrane durable for a long storage period, because we observed that dried CHP nanogel membrane was also effective in the same bone defect model (authors' unpublished data). Second, enhancement of mechanical strength of the membrane is absolutely required. The present CHP nanogel membrane is strong enough to cover over a relatively small bone defect; however, it is obviously too weak to be applied for vertical or horizontal bone augmentation. Combining CHP nanogel membrane with biodegradable polymer would solve this problem.

5. Conclusion

The present results indicate that novel CHP nanogel cross-linking membrane would be potentially effective as a GBR membrane.

Acknowledgements

We greatly appreciate the help of Dr Tomoko Nagayama, Dr Jia Hao, Dr Reena Rodriguez, Dr Warunee Pluemsakunthai and Dr